TECHNOLOGY AND APPLICATIONS

High accuracy photopyroelectric investigation of dynamic thermal parameters of Fe_3O_4 and $CoFe_2O_4$ magnetic nanofluids

D. Dadarlat · C. Neamtu · M. Streza · R. Turcu · I. Craciunescu · D. Bica · L. Vekas

Abstract The suitability of the photopyroelectric (PPE) calorimetry in measuring the thermal parameters of nanofluids was demonstrated. The main advantages of the method (concerning nanofluids) as compared to classical calorimetric techniques are: high sensitivity and small amount of sample required. The thermal diffusivity and effusivity of some nanofluids based on Fe_3O_4 and $CoFe_2O_4$ type of nanoparticles (mean diameter 6.5 nm) were investigated by using two PPE detection configurations (back and front). In both cases, the information is contained in the phase of the PPE signal. Due to the high accuracy of the results (within ±0.5%) thermal diffusivity was found to be particularly sensitive to changes in relevant parameters of the nanofluid as carrier liquid, type and concentration of nanoparticles.

Nomenclature
k Thermal conductivity
R Reflection coefficient of the thermal wave
e Thermal effusivity
f Chopping frequency
a Reciprocal of the thermal diffusion length
C Volume specific heat

Greek symbols
α Thermal diffusivity
Θ Phase of the photopyroelectric signal
μ Thermal diffusion length

Subscripts
m Material
p Pyroelectric sensor
w Window
abs Absolute value

D. Dadarlat · C. Neamtu · M. Streza (✉) ·
R. Turcu · I. Craciunescu
National R&D Institute for Isotopic and Molecular Technologies, 65-103 Donath St., P.O. Box 700, 400293 Cluj-Napoca, Romania
e-mail: streza.mihaela@gmail.com

D. Bica · L. Vekas
Laboratory of Magnetic Fluids, Romanian Academy – Timisoara Branch, 24 Mihai Viteazul St., Timisoara, Romania

Introduction

Ferrofluids represent a special category of smart nanomaterials, consisting of stable dispersions of magnetic nanoparticles in different liquid carriers. Stabilization of ferrofluids implies various procedures depending on the nature of the liquid. The most stable ferrofluids are known among those based on organic

non-polar solvents, in which case the presence of a single layer of surfactant on the surface of magnetic nanoparticles is enough to avoid the particles aggregation. We have to point out that biological applications of ferrofluids require stable polar ferrofluids especially based on water. Water-based magnetic nanofluids are currently investigated to develop new magnetically controlled drug delivery systems and magnetic separation methods of biomaterials.

If the magnetic properties of the magnetic nanofluids are the subject of an intensive study, there are rather few data in literature concerning their thermal properties (Kebilinski et al. 2005). Normally, the thermal properties of the magnetic nanofluids must depend on the composition of the nanofluid (type of nanoparticles, surfactant and carrier fluid), concentration, nanoparticles' size, etc. Even more, the values of the static and dynamic thermal parameters and their temperature behaviour (phase transitions, for example) are correlated with structural changes and/or with the dynamics of various processes (drug delivery, for example) occurring inside the nanofluid.

On the other side, the few calorimetric data from literature indicate sometimes drastic changes of the thermal conductivity as a function of nanoparticles' size—case of Cu nanoparticles or carbon nanotubes immersed in ethylene glycol, for example (Eastman et al. 2001; Choi et al. 2001).

The limited number of thermal data concerning magnetic nanofluids can be due, in principle, to the fact that the classical calorimetric techniques do not fit properly to nanofluids: some of the methods are time consuming, they are not always very precise, and usually they need calibration and especially a large quantity of sample. Even more, any classical calorimetric technique is able to measure *only one* thermal parameter, usually the static one (specific heat), or the thermal conductivity.

In the last years, two photopyroelectric (PPE) calorimetric configurations (i.e. "back" and "front", respectively) have been applied for investigating the behaviour of thermal parameters of condensed matter samples (Chirtoc et al. 1997; Chirtoc and Mihailescu 1989).

In principle, in the PPE technique, the temperature variation of a sample, exposed to a modulated radiation is measured with a pyroelectric sensor. In the most general case, the complex PPE signal depends on all optical and thermal parameters of the layers of the detection cell, but after some mathematical approximations, one can obtain results in which the amplitude or the phase of the signal depend on one or, in a simple way, on two of the sample's related thermal parameters. In these special cases of experimental interest, the information is usually contained in the amplitude of the signal, the phase being often constant. However, sometimes, the phase of the PPE signal also contains information, and it refers to either thermal diffusivity or effusivity of the sample (Mandelis and Zver 1985; Dadarlat et al. 1995).

In the *back configuration*, the most convenient PPE particular case, largely used in order to find the values of the *thermal diffusivity*, requests thermally thick sample and sensor and optically opaque sample. In this configuration, a modulated light impinges on the front surface of a sample, and a pyroelectric sensor, situated in good thermal contact with the sample's rear side, measures the heat developed in the sample due to the absorption of radiation. In order to find the thermal diffusivity of a given sample, the phase of the PPE signal can be measured, by performing either a frequency or a thickness scan (Marinelli et al. 1992, 1994; Balderas et al. 2000). Recently, it has been demonstrated that the methodology based on sample's thickness scan leads to very accurate and reproducible values for the thermal diffusivity, due to the possibility of precisely controlling the sample's thickness variation (Shen and Mandelis 1995; Shen et al. 1998; Delenclos et al. 2007).

In the *front configuration*, the radiation impinges on the front surface of the sensor, and the sample, in good thermal contact with its rear side, acts as a heat sink (Dadarlat et al. 1990). Recently, this front configuration was used to measure the *thermal effusivity* of some (semi)liquids. The experimental conditions (chopping frequency, number and geometrical thickness of the layers of the detection cell) were set up in such a way that the information (the value of the thermal effusivity) is contained in the phase of the signal (Neamtu et al. 2006; Dadarlat and Neamtu 2006).

Consequently, one can obtain through the PPE calorimetric techniques, *all static and dynamic thermal parameters* (by directly measuring two independent ones). It is important to note, the PPE calorimetry is in fact able to directly measure the "fundamental"

thermal parameters (contained in the thermal diffusion equation and its solution), the thermal diffusivity and effusivity, and then derive the remaining two, thermal conductivity and specific heat. We have also to stress on the fact that the PPE calorimetry seems to be particularly suitable for nanofluids due to the small amount of sample required (max. 0.2–0.3 mL).

The purpose of the article is use of high accuracy PPE calorimetry (in the two configurations previously described) in order to directly measure the thermal diffusivity and effusivity of some nanofluids based on Fe_3O_4 and $CoFe_2O_4$ nanoparticles. The suitability of a study of the changes of these thermal parameters as a function of some relevant parameters of the nanofluid (carrier liquid, type and concentration of nanoparticles) is now possible due to the recent increase of the sensitivity of the PPE investigations (Delenclos et al. 2007).

Theory

The theory of the two configurations (including the approximations for each particular case), together with the schematic diagrams of the detection cells were presented elsewhere (Neamtu et al. 2006; Dadarlat and Neamtu 2006; Delenclos et al. 2002; Hadj Sahraoui et al. 2003).

We give here only the resulting equations for the phase of the PPE signal.

Back configuration

In the particular case when the sensor is thermally thick and the sample is optically opaque, the expression for the phase of the PPE signal in the back configuration is given by:

geometrical thickness of the layer of the detection cell, e represents the thermal effusivity and a is the reciprocal of the thermal diffusion length ($a = 1/\mu$), respectively. The thermal diffusion length depends on the thermal diffusivity α and chopping frequency f as: $\mu = (\alpha/\pi f)^{1/2}$. The symbols "m", "p" and "w" refer to material (sample), pyroelectric sensor and window, respectively (Delenclos et al. 2007; Dadarlat et al. 1990; Neamtu et al. 2006; Dadarlat and Neamtu 2006; Delenclos et al. 2002).

Due to the recent improvements in the thickness control of liquid samples, we select for this configuration the thermal-wave-resonator-cavity (TWRC) alternative: a sample's thickness scan at constant copping frequency. A mathematical simulation of (1) indicates that, for a scanning range larger than about 3 μ_m, the behaviour of the phase of the PPE signal is linear as a function of sample's thickness, and the thermal diffusivity can be calculated as (Delenclos et al. 2007):

$$\alpha_m = \frac{\pi f L_{abs}^2}{\Theta_{abs}^2} \qquad (2)$$

where L_{abs} and Θ_{abs} represent the absolute values of the sample's thickness and PPE signal phase.

As a conclusion of this section, the thermal diffusivity can be obtained by performing a sample's thickness scan of the phase of the PPE signal.

Front configuration

In the front configuration, with opaque sensor and thermally thick sensor and sample, the phase of the PPE signal is given by:

$$\tan \Theta = \frac{(1 + R_{mp}) \exp(-x) \sin(x)}{1 - (1 + R_{mp}) \exp(-x) \cos(x)} \qquad (3)$$

$$\Theta = - \arctan \left[\frac{\sin(x) - R \exp(-2x)[\sin(x)\cos(2x) - \cos(x)\sin(2x)]}{\cos(x) - R \exp(-2x)[\sin(x)\sin(2x) + \cos(x)\cos(2x)]} \right] \qquad (1)$$

where x = $a_m L_m$; $R = R_{mw} R_{mp}$; $b_{jk} = e_j/e_k$.

In Eq. 1 R_{jk} represents the reflection coefficient of the thermal wave at the 'jk' interface, L is the

From (3), for a given frequency, one can calculate R_{mp} and then derive the sample's effusivity e_m, according to the following relationship:

$$\frac{e_{\mathrm{m}}}{e_{\mathrm{p}}} = \frac{1 + R_{\mathrm{mp}}}{1 - R_{\mathrm{mp}}} \qquad (4)$$

Equations 3 and 4 indicate that sample's thermal effusivity can be directly measured by performing a frequency scan of the phase of the PPE signal.

We mention also that the thermal diffusivity and effusivity are related to the other thermal parameters (the volume specific heat C and thermal conductivity k) by:

$$k = C\alpha ; \quad e = (Ck)^{1/2} \qquad (5)$$

As a conclusion of this theoretical section, a combined "back-front" PPE investigation can lead to accurate values for two dynamic thermal parameters, thermal diffusivity and effusivity (the remaining two can be derived using (5)). The main particularities of the method responsible for the high accuracy of the results are: (i) the information is contained in the phase of the PPE signal; (ii) the values of the thermal parameters are results of fitting procedures (and not isolated measured data); (iii) the recent designed PPE detection cells allow for very accurate control of chopping frequency and sample's thickness variation.

Experimental

A standard PPE calorimetric line was used for investigations (Dadarlat et al. 1995). The radiation source was a 30 mW HeNe laser, chopped by an acousto-optical modulator. The signal from a 500 μm thick LiTaO$_3$ pyroelectric sensor was processed with a SR 830 lock-in amplifier.

The detection cell in the front configuration was presented elsewhere (Dadarlat et al. 1995; Dadarlat et al. 1990; Hadj Sahraoui et al. 2003; Longuermart et al. 2002). The liquid sample is accommodated in a glass cylinder, 5 mm thick, glued on the rear side of the sensor. It is to point out that the cell can be filled and the sample removed without moving the sensor. The frequency scan was performed in the 1–25 Hz frequency range, with a step of 0.5 Hz. In this frequency range, both the sensor and the sample are thermally thick. The optical opacity of the sensor was ensured by its front (Cr–Au) electrode. In order to eliminate parameters difficult to be estimated experimentally (e.g. incident radiation power density, radiation to heat conversion efficiency, thermal and

electrical time constants of the electrical circuit), the PPE phase was normalized to the one obtained with air instead of sample; the obtained normalized phase satisfies (3). The accuracy of the results for thermal effusivity investigations are ±1%.

The detection cell, in the back configuration was also described before (Delenclos et al. 2007; Dadarlat et al. 1990; Neamtu et al. 2006; Dadarlat and Neamtu 2006; Delenclos et al. 2002)

The radiation source was modulated at 12 or 24 Hz, respectively, by an acousto-optical modulator, driven from the internal oscillator of the lock-in amplifier, used also for signal processing. The value of the frequency was selected to satisfy the conditions imposed for the validity of (2), and was kept constant with a precision better than 0.1 mHz. The modulated radiation passed through a 1.2 mm thick quartz window situated on a rotating table, and was absorbed by an opaque 0.1 μm thick titanium layer, deposited on the rear side of the window. The liquid sample accommodated the space between the sensor and the titanium layer. The sample's thickness variation was performed with a step of 0.03 μm (9062M-XYZ-PPP Gothic-Arch-Bearing picomotor). This high accuracy of sample's thickness control (the best reported until now) leads to an accuracy of the measured thermal diffusivity values better than ±0.5%. The sample's thickness control and data acquisition were performed with adequate software.

In both configurations, a computer was used for data acquisitions. The signal/noise ratio (in the linear range of the thickness scan) was better than 1000.

The magnetic nanofluids were prepared by a two-stage process, involving first the synthesis of magnetic nanoparticles, followed by the stabilization/dispersion of surface covered magnetic nanoparticles in various non-polar and polar carrier liquids (Vekas et al. 2007).

Fe$_3$O$_4$ nanoparticles were synthesized through coprecipitation of Fe^{3+}, Fe^{2+} ions in solution, with NH$_4$OH (or NaOH) in excess. The temperature was maintained at 80–82 °C, in order to obtain only magnetite nanoparticles and to ensure optimal conditions for chemisorption of the surfactant. In the case of decahydronaphtalene (DHNA; non-polar) carrier the magnetite nanoparticles were covered with oleic acid monolayer (Vekas et al. 2006). For the water-based samples used in this work, with magnetite or cobalt-ferrite nanoparticles, double-layer sterical
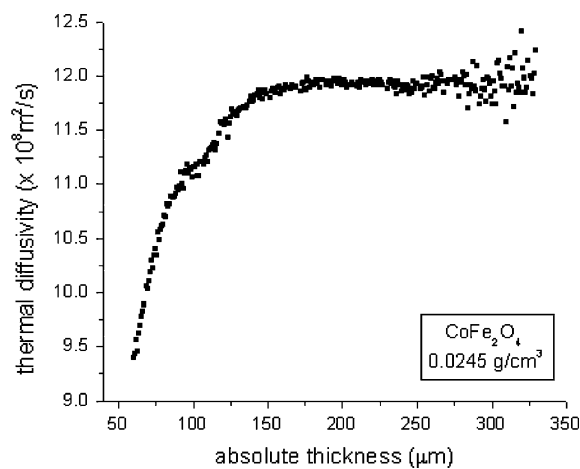
stabilization procedure was applied (Bica et al. 2002), using technical grade dodoecyl-benzen-sulphonic acid. A second layer of surfactant DBS was physically adsorbed on the first chemisorbed layer of DBS in order to obtain stable water based magnetic nanofluid samples (Vekas et al. 2006).

The details of stabilization/dispersion of magnetite nanoparticles in various carriers to obtain stable magnetic fluids, such as pH and temperature or elimination of excess surfactant are given elsewhere (Vekas et al. 2006, 2007; Bica et al. 2002). Generally, the nature of the surfactants, used for nanoparticles stabilization, influences their size distribution. For the purpose of this article, we selected nanoparticles stabilized with DBS + DBS and with OA, case when the mean size of the nanoparticles is similar, about 6.5 nm (Vekas et al. 2007). In such a way, the nanoparticles' size will not interfere in the influence of the carrier liquid, type and concentration of nanoparticles, on the dynamic thermal parameters of the nanofluid.

Results and discussion

A typical behaviour of the thermal diffusivity as a function of sample's thickness, for a water-based nanofluid with $CoFe_2O_4$ type of nanoparticles, stabilized by a double layer of surfactants DBS + DBS is presented in Fig. 1.

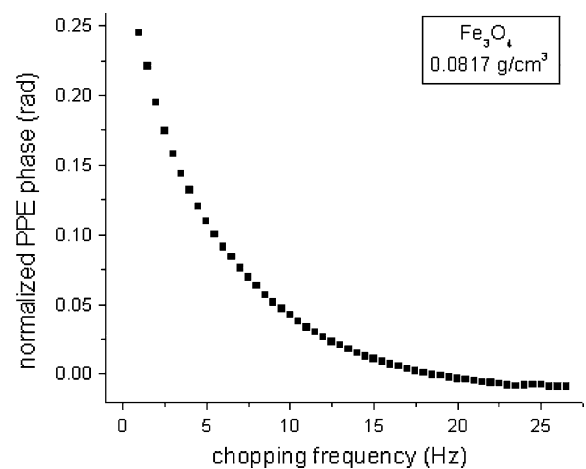Figure 1 indicates that the thickness scan of the thermal diffusivity presents three different regions (Delenclos et al. 2007). As predicted by (1), the region of interest is the thermally thick regime for the sample ($3\mu_m < L_m < 4 \div 5\mu_m$), where the linear, horizontal behaviour gives the value of the thermal diffusivity. As an indication, for a liquid with a thermal diffusivity of about 12×10^{-8} m^2 s^{-1}, at 24 Hz chopping frequency, the thermal diffusion length is about procedure of data analysis (Delenclos et al. 2007). The first step is to use the measured 40 μm.

Figure 1 is in fact the result of a rather complicated "relative phase versus relative thickness" data in order to find an initial approach for the thermal diffusivity. With this "rough" value of the thermal diffusivity, one can calculate the thermal diffusion length. Using a calibration measurement for the initial offset of the phase of the signal (by directly irradiating the empty sensor), one can also obtain the absolute value of the phase of the signal, (Θ_{abs}), and a "rough" value of the absolute sample's thickness. The next step is to use the obtained data, to locate the linear (in general 3–5μ_m) region of the thickness scan, and to perform a fit of the experimental data in this region, in order to obtain improved values for the thermal diffusivity and L_{abs}. The correct value of the thermal diffusivity will be obtained by using a fitting procedure: the best fit will be selected by minimizing the relative error of thermal diffusivity found with (2), as compared to the best fit value of the linear part of the curve, with L_{abs} as a fit parameter.

Figure 2 presents a typical frequency scan of the phase of the PPE signal, in the front configuration.

Fig. 1 Typical thickness scans of the thermal diffusivity (as calculated with (2)) for a water-based nanofluid with $CoFe_2O_4$ type of nanoparticles, concentration 0.0245 g cm^{-3}

Fig. 2 Typical frequency scan of the phase of the PPE signal for a water-based nanofluid with Fe_3O_4 type of nanoparticles, concentration 0.0817 g cm^{-3}
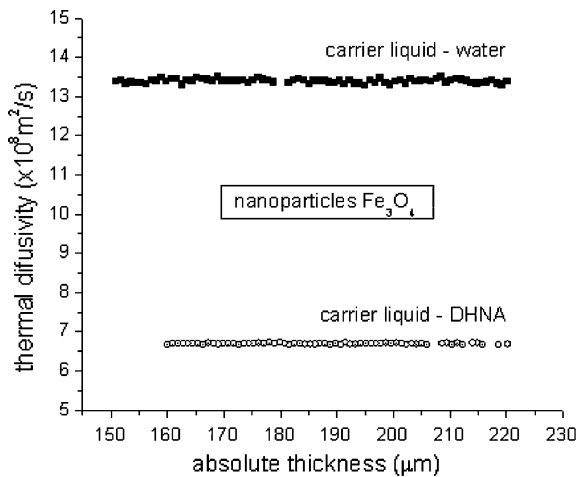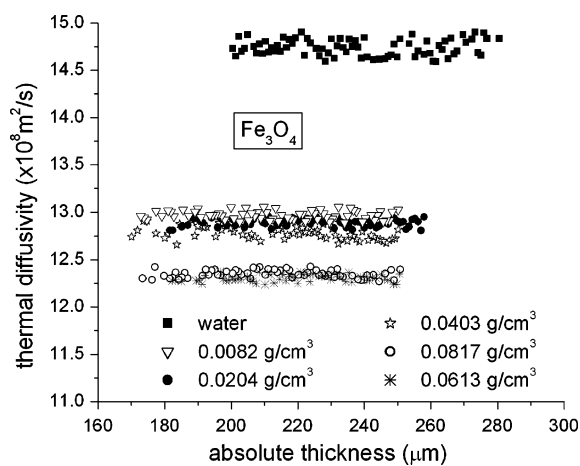
Fig. 3 Typical thickness scans of the thermal diffusivity, in the thermally thick regime for the sample, for nanofluids with Fe_3O_4 nanoparticles, stabilized in different carrier liquids: water and DHNA, respectively

The thermal effusivity can be derived by fitting these experimental data with (3): the correct value of the thermal effusivity optimizes the fit.

In the following, several nanofluid samples with different relevant parameters (carrier liquid, type and concentration of nanoparticles) were investigated, in order to test the suitability of the PPE calorimetry for such type of investigations.

Figure 3 presents the thickness scan of the thermal diffusivity, obtained for nanofluids based on Fe_3O_4


Fig. 4 Results of the thickness scans, obtained for the thermal diffusivity for water-based nanofluids with Fe_3O_4 nanoparticles at different concentrations
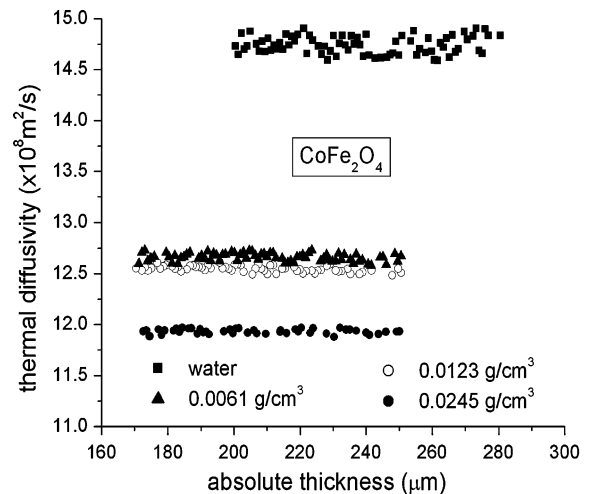

Fig. 5 Results of the thickness scans, obtained for the thermal diffusivity for water-based nanofluids with $CoFe_2O_4$ nanoparticles at different concentrations

nanoparticles, but with different carrier fluid, water and DHNA, respectively.

Figures 4 and 5 display thickness scans of the thermal diffusivity for water based nanofluids with different nanoparticles (Fe_3O_4 and $CoFe_2O_4$) and, for each type of nanoparticles, with different concentrations.
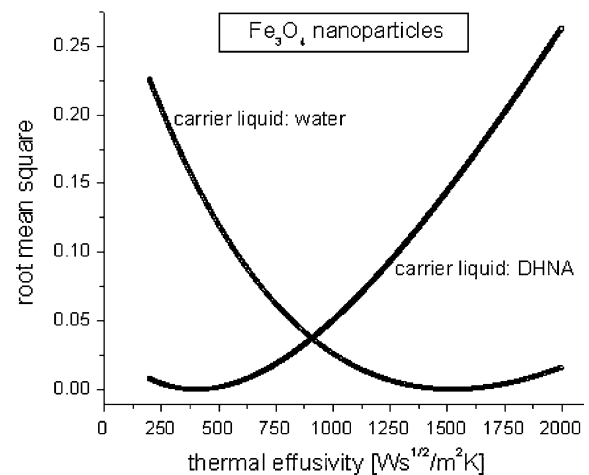
Fig. 6 The root-mean-square (rms) of the fit performed with (3) on the experimental data (PPE phase as a function of chopping frequency), with sample's thermal effusivity as a fit parameter. The minimum of the curve indicates the correct value of the thermal effusivity. Sample: nanofluid with Fe_3O_4 nanoparticles and different liquid carrier (water and DHNA, respectively)
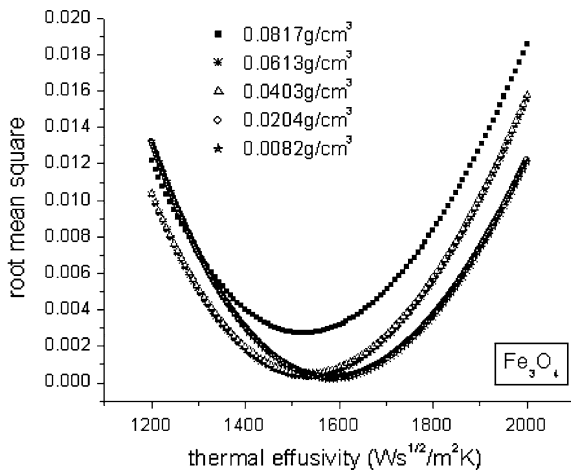
Fig. 7 Similar with Fig. 6. Sample: water-based nanofluid with Fe_3O_4 nanoparticles
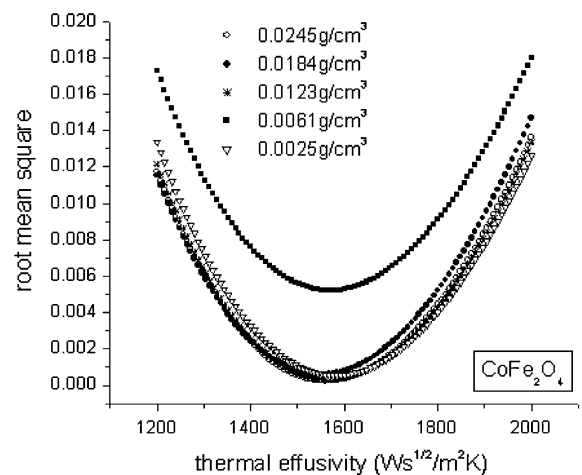
Fig. 8 Similar with Fig. 6. Sample: water-based nanofluid with $CoFe_2O_4$ nanoparticles

Figures 3–5 indicate that thermal diffusivity is a sensitive thermal parameter to changes of main nanofluids' parameters (carrier liquid, type and concentration of nanoparticles), and also that the PPE calorimetry in the TWRC configuration is enough accurate for such type of investigations.

Figures 6–8 present the optimization of the fits performed in order to calculate the thermal effusivity. The same nanofluid samples were used for investigations. The correct value of the thermal effusivity minimizes the root mean square of the fit performed with (3). A "noisy" measurement was added to the graphs for each type of nanofluid, in order to indicate the limits of the accuracy of our investigations.

As one can see, the thermal effusivity depends also on the main parameters of the nanofluid, but it is less

sensitive than thermal diffusivity. The changes of the thermal effusivity as a function of liquid carrier are clearly detected, but the changes as a function of type of nanoparticles and concentration lie somewhere within the precision of the measurement, $\pm 1\%$.

The synthesis the results of the measured data, including the accuracy for each measurement are presented in Table 1.

Conclusions

The PPE calorimetry, in two detection configurations was used in order to directly measure the thermal diffusivity and effusivity of some nanofluids. Due to the high accuracy of the results and the small amount

Table 1 The values of the thermal diffusivity and effusivity of the investigated samples, together with the accuracy of each measurement

Fe_3O_4					$CoFe_2O_4$				
Concentration $(g\ cm^{-3})$	Thermal diffusivity $(10^8\ m^2\ s^{-1})$	Standard deviation $(10^8\ m^2\ s^{-1})$	Thermal effusivity $(W\ s^{1/2}\ m^{-2}\ K^{-1})$	Root mean square (10^4)	Concentration $(g\ cm^{-3})$	Thermal diffusivity $(10^8\ m^2\ s^{-1})$	Standard deviation $(10^8\ m^2\ s^{-1})$	Thermal effusivity $(W\ s^{1/2}\ m^{-2}\ K^{-1})$	Rms (10^4)
0	14.743	±0.087	1584	2.63	0	14.743	±0.087	1584	2.63
0.0082	12.957	±0.058	1584	2.18	0.0025	12.642	±0.043	1581	5.49
0.0204	12.886	±0.040	1583	2.89	0.0061	12.650	±0.046	1570	52.1
0.0403	12.759	±0.081	1533	4.96	0.0123	12.541	±0.045	1566	2.73
0.0613	12.303	±0.044	1534	3.07	0.0184	11.995	±0.044	1550	6.13
0.0817	12.346	±0.049	1525	27.2	0.0245	11.921	±0.036	1560	2.36

of sample required, the PPE technique seems to be particularly suitable for investigating thermal properties of magnetic nanofluids. Both thermal diffusivity and effusivity are influenced by structural parameters of nanofluids as carrier liquid, type and concentration of nanoparticles, with a special notice for thermal diffusivity.

We have to mention that the high accuracy of the results is due to the recent development of the PPE calorimetric techniques, especially the high accuracy in controlling sample's thickness in the TWRC configuration (30 nm step).

The remaining thermal parameters (thermal conductivity and volume specific heat) can be easily calculated using (5).

Due to its features, we consider that the PPE calorimetry became a promising alternative to classical techniques, concerning magnetic nanofluids.

For this study, nanoparticles with similar size were selected; work is in progress with studies of the influence of the nanoparticles size on the thermal parameters of magnetic nanofluids.

References

Balderas-Lopez JA, Mandelis A, Garcia JA (2000) Thermal-wave resonator cavity design and measurements of the thermal diffusivity of liquids. Rev Sci Instrum 71:2933–2937

Bica D, Vekas L, Rasa M (2002) Preparation and magnetic properties of concentrated magnetic fluids on alcohol and water carrier liquids. J Magn Magn Mater 252:10–12

Chirtoc M, Mihailescu G (1989) Theory of the photopyroelectric method for investigation of optical and thermal materials properties. Phys Rev B 40:9606–9617

Chirtoc M, Dadarlat D, Bicanic D, Antoniow JS, Egee M (1997) Applications of photothermal calorimetry in agriculture, medicine and environmental sciences. In: Mandelis A, Hess P (eds) Progress in photothermal and photoacoustic science and technology. SPIE Optical Engineering Press, Belingham, USA, pp 185–257

Choi SUS, Zhang ZG, Yu W, Lockwood FE, Grulke EA (2001) Anomalous thermal conductivity enhancement in nanotube suspension. Appl Phys Lett 79:2252–2254

Dadarlat D, Neamtu C (2006) Detection of molecular associations in liquids by photopyroelectric measurements of thermal effusivity. Meas Sci Technol 17:3250–3254

Dadarlat D, Chirtoc M, Neamtu C, Candea R, Bicanic D (1990) Inverse photopyroelectric detection method. Phys Stat Sol (a) 121:K231–K234

Dadarlat D, Bicanic D, Visser H, Mercuri F, Frandas A (1995) Photopyroelectric method for determination of thermophysical parameters and detection of phase transitions in fatty acids and triglycerides. Part I: principles, theory and instrumentational concepts. J Am Oil Chem Soc 74:273–281

Delenclos S, Chirtoc M, Hadj Sahraoui A, Kolinsky C, Buisine JM (2002) Assessment of calibration procedures for accurate determination of thermal parameters of liquids and their temperature dependence using the photopyroelectric method. Rev Sci Instrum 73:2773–2780

Delenclos S, Dadarlat D, Houriez N, Longuermart S, Kolinsky C, Hadj Sahraoui A (2007) On the accurate determination of thermal diffusivity of liquids by using the photopyroelectric thickness scanning method. Rev Sci Instrum 78:024902

Eastman JA, Choi SUS, Li S, Yu W, Thomson LJ (2001) Anomalously increased effective thermal conductivities of ethylene glycol-based nanofluids containing copper nanoparticles. Appl Phys Lett 78:718–720

Kebilinski P, Eastman JA, Cahill DG (2005) Nanofluids for thermal transport. Mater Today 8:36–44

Longuermart S, Quiroz AG, Dadarlat D, Hadj Sahraoui A, Kolinsky C, Buisine JM, Correa da Silva E, Mansanares AM, Filip X, Neamtu C (2002) An application of the front photopyroelectric technique for measuring the thermal effusivity of some foods. Instr Sci Technol 30:157–165

Mandelis A, Zver M (1985) Theory of the photopyroelectric effect in solids. J Appl Phys 57:4421–4430

Marinelli M, Zammit U, Mercuri F, Pizzoferrato R (1992) High-resolution simultaneous photothermal measurements of thermal parameters at a phase transition with the photopyroelectric technique. J Appl Phys 72:1096–1100

Marinelli M, Mercuri F, Zammit U, Pizzoferrato R, Scudieri F, Dadarlat D (1994) Photopyroelectric study of specific heat, thermal conductivity and thermal diffusivity of Cr_2O_3 at the Neel transition. Phys Rev B 49:9523–9532

Neamtu C, Dadarlat D, Chirtoc M, Hadj Sahraoui A, Longuemart S, Bicanic D (2006) Evidencing molecular associations in binary liquid mixtures via photothermal measurements of thermophysical parameters. Instr Sci Technol 34:225–232

Sahraoui AH, Longuermart S, Dadarlat D, Delenclos S, Kolinsky C, Buisine JM (2003) Analysis of the photopyroelectric signal for investigating thermal parameters of pyroelectric materials. Rev Sci Instrum 74:618–623

Shen J, Mandelis A (1995) Thermal-wave resonator cavity. Rev Sci Instrum 66:4999–5005

Shen J, Mandelis A, Tsai H (1998) Signal generation mechanism, intercavity – gas thermal diffusivity temperature dependence and absolute infrared emissivity measurements in a thermal-wave resonant cavity. Rev Sci Instrum 69:197–203

Vekas L, Bica D, Marinica O (2006) Magnetic nanofluids stabilized with various chain length surfactants. Rom Rep Phys 58:257–267

Vekas L, Bica D, Avdeev MV (2007) Magnetic nanoparticles and concentrated magnetic nanofluids: synthesis, properties and some applications. China Particuol 5:43–51